11-30-2012

Septin Phosphorylation and Coiled-Coil Domains Function in Cell and Septin Ring Morphology in the Filamentous Fungus Ashbya Gossypii

Rebecca A. Meseroll
Dartmouth College

Patricia Occhipinti
Dartmouth College

Amy S. Gladfelter
Dartmouth College

EC
Journals.ASM.org

Septin Phosphorylation and Coiled-Coil Domains Function in Cell and Septin Ring Morphology in the Filamentous Fungus *Ashbya gossypii*

Rebecca A. Meseroll,* Patricia Occhipinti, Amy S. Gladfelter

Dartmouth College, Department of Biological Sciences, Dartmouth College, Hanover, New Hampshire, USA

Septins are a class of GTP-binding proteins conserved throughout many eukaryotes. Individual septin subunits associate with one another and assemble into heteromeric complexes that form filaments and higher-order structures *in vivo*. The mechanisms underlying the assembly and maintenance of higher-order structures in cells remain poorly understood. Septins in several organisms have been shown to be phosphorylated, although precisely how septin phosphorylation may be contributing to the formation of high-order septin structures is unknown. Four of the five septins expressed in the filamentous fungus, *Ashbya gossypii*, are phosphorylated, and we demonstrate here the diverse roles of these phosphorylation sites in septin ring formation and septin dynamics, as well as cell morphology and viability. Intriguingly, the alteration of specific sites in Cdc3p and Cdc11p leads to a complete loss of higher-order septin structures, implicating septin phosphorylation as a regulator of septin structure formation. Introducing phosphomimetic point mutations to specific sites in Cdc12p and Shs1p causes cell lethality, highlighting the importance of normal septin modification in overall cell function and health. In addition to discovering roles for phosphorylation, we also present diverse functions for conserved septin domains in the formation of septin higher-order structure. We previously showed the requirement for the Shs1p coiled-coil domain in limiting septin ring size and reveal here that, in contrast to Shs1p, the coiled-coil domains of Cdc11p and Cdc12p are required for septin ring formation. Our results as a whole reveal novel roles for septin phosphorylation and coiled-coil domains in regulating septin structure and function.

Septins are cytoskeletal proteins first described as cell division cycle mutants in yeast (1). Since their initial discovery, the septins have been shown to be conserved throughout many eukaryotes (2, 3), where they participate in diverse cellular functions, including cytokinesis, apoptosis, membrane compartmentalization, and acting as scaffolds for other signaling proteins (4–9). Misexpression or dysfunction of the septins in humans has been correlated with neurological disorders, such as Parkinson's and Alzheimer's diseases (10, 11), and various cancer types (12).

Septins form heteromeric complexes that assemble into filaments and different higher-order structures in cells (13, 14), and septin organization into these assemblies is tightly linked to function (15). *In vitro*, purified septins form nonpolar heteromeric complexes that can self-assemble into long, paired filaments under low-salt conditions (16, 17). Under high-salt conditions that normally inhibit septin filament polymerization, the addition of phosphatidylinositol-4,5-bisphosphate (PIP_2) membranes allows for the assembly of septins into a crossed network of filaments (18), indicating that membranes can promote septin polymerization. In cells, septins organize into a variety of higher-order structures, including rings, gauzes, and bars (11, 19, 20). These structures are frequently associated with the cell cortex, and their organization at specific times in specific locations are required for normal septin function. The exact mechanisms governing septin organization into complexes, filaments, and higher-order structures remain mysterious. How are septins instructed to form the varied higher-order structures that we observe in cells? What controls the dynamics of septin assemblies? How does septin organization influence septin function?

To address these questions, we used the filamentous fungus, *Ashbya gossypii*, as a model organism. Septins in *Ashbya* organize into three distinct, cortically associated structures: rings at the branch sites, rings throughout the inter-region of hyphae, and diffuse clouds at the hyphal tips (19). In contrast to the septin collars that form at the mother-bud neck of the budding yeast *Saccharomyces cerevisiae*, which assemble and disassemble in a cell cycle-dependent manner, septin rings in *Ashbya* persist over many hours, independent of the cell cycle (19). *Ashbya* expresses the same five vegetative septins as yeast (Cdc3p, Cdc10p, Cdc11p, Cdc12p, and Shs1p/Sep7p), all of which are required for septin ring formation (19).

It has been demonstrated in many systems, from yeast to mammals, that septins are posttranslationally modified, and these modifications function in septin organization and activity (21–30). Phosphorylation is by far the most common modification found on septins, and septins rely upon kinases to achieve normal structure and function (19, 22, 24, 25, 27, 28, 31, 32). We previously identified two *Ashbya* kinases (Elm1p and Gin4p) that are required for assembly of subset of septin rings (19) and subsequently identified multiple phosphorylation sites on the septin Shs1p (25). Changing the phosphorylation sites to nonphosphor-

Received 12 September 2012 **Accepted** 23 November 2012

Published ahead of print 30 November 2012

Address correspondence to Amy S. Gladfelter, amy.gladfelter@dartmouth.edu.

* Present address: Rebecca A. Meseroll, Laboratory of Cell and Molecular Biology, National Institute of Diabetes and Digestive and Kidney Diseases, National Institutes of Health, Bethesda, Maryland, USA.

Supplemental material for this article may be found at http://dx.doi.org/10.1128/EC.00251-12.

doi:10.1128/EC.00251-12

TABLE 1 *Ashbya* strains used in this study

Strain	Relevant genotype[a]	Source or reference
Wild type	Δ*leu2*Δ*thr4*	35
AG124	Ag*SHS1-GFP-GEN3*	36
AG384.1	Ag*Cdc11a-GFP-GEN3*	This study
AG413.2	Ag*Cdc3-GFP-GEN3*	This study
AG436.1	Ag*Cdc12-GFP-GEN3*	This study
AG442.1	pAGB088 [pAg *Shs1-GFP-GEN3*]	25
AG495.1	Ag*CDC11a-TAP-GEN3*	25
AG529.1	pAGB383 [pAG *Cdc3 S91A-GFP-GEN3*]	This study
AG531.1	pAGB384 [pAG *Cdc3 S496D-GFP-GEN3*]	This study
AG533.1	pAGB386 [pAG *Cdc11a S314D-GFP-GEN3*]	This study
AG537.1	pAGB378 [pAG *Shs1 9D-GFP-GEN3*]	This study
AG652.1	Ag*Cdc12*Δ*CC-GFP-GEN3**	This study
AG656.1	Ag*Cdc11a*Δ*CC-GFP-GEN3**	This study
AG657.1	Ag*Shs1*Δ*CC-Cdc11aCC-GFP-GEN3*	This study
AG688.1	Ag*Cdc3 S91D-GFP-GEN3*	This study
AG669.2	Ag*Cdc11a S314A-GFP-GEN3*	This study
AG671.1	Ag*Cdc12 S5A S8A-GFP-GEN3*	This study
AG672	Ag*Cdc12 S323A-GFP-GEN3**	This study
AG674	pAGB470 [pAg *Cdc12 S5D-GFP-GEN3*]	This study

[a] With the exception of plasmidic strains (in brackets) and heterokaryotic strains (marked with asterisks), all analyzed mycelia were homokaryotic (all nuclei have the same genotype).

ylatable alanine resulted in an increased steady-state concentration of septin at the inter-region rings and a trend toward decreased septin dynamics. When phosphomimetic mutations are introduced to *SHS1* at its endogenous locus, the allele is lethal. In addition, the coiled-coil domain that lies amid the Shs1 phosphorylation sites is necessary to limit septin ring size and dynamics. These results demonstrated the requirement for phosphorylation and conserved domains in septin organization and prompted examination of the functions of phosphorylation of the remaining *Ashbya* septins. The data presented here reveal requirements for septin phosphorylation and coiled-coil domains in septin organization into higher-order structures, septin dynamics, cell morphology, and even cell viability.

MATERIALS AND METHODS

Growth conditions and strain construction. *A. gossypii* media, culturing, and transformation protocols are described previously (33, 34). The strains generated and used in the present study are described in Table 1. The plasmids used in this study are listed in Table 2. The oligonucleotide primers are listed in Table 3. All single point mutations were made on full-length plasmids using a QuikChange II XL site-directed mutagenesis kit (Agilent Technologies, Santa Clara, CA). All gel purifications were performed with the QIAquick gel extraction kit (Qiagen, Valencia, CA).

(i) Cdc3 point mutation strain construction. AGB221 was made by cotransforming yeast with *GFP-GEN3* amplified from AGB141 using the primer pair AGO589/AGO505 with AGB127. The plasmid was verified by digest with EcoRI and KpnI, followed by sequencing with primers AGO98, AGO199, AGO472, AGO520, AGO521, and AGO539. The gel-purified 4,167-bp product of AGB221 digested with MluI and NotI was transformed into wild-type *Ashbya* strain ΔIΔt to obtain strain AG413.2, which was verified by PCR using the oligonucleotides AGO98, AGO199, AGO315, and AGO405. AGB383 was made using primer pair AGO940/AGO941 on AGB380 and verified by sequencing with the primers AGO101 and AGO954. AGB383 was transformed into ΔIΔt to obtain AG529.1. AGB362 was obtained using primer pair AGO942/AGO943 on AGB221, verified by digestion with BclII and BciVI, and sequenced with the primer AGO954. AGB362 was digested with XhoI and NotI and transformed into ΔIΔt to obtain AG688.1, which was verified by PCR using the oligonucleotide pairs AGO954/AGO101 (followed by digest with BglII to confirm presence of the point mutation), AGO199/AGO5, AGO471/AGO315, and AGO98/AGO315. AGB384 was obtained by using the primer pairs AGO940/AGO941 on AGB380 and verified with the sequencing primers AGO199 and AGO202. AGB384 was transformed into ΔIΔt to obtain AG531.1.

(ii) Cdc11 point mutation strain construction. AGB214 was made by cotransforming yeast with *GFP-GEN3* amplified from AGB141 using the primer pair AGO540/AGO541 with AGB125. The plasmid was verified with AflII and BglII, followed by sequencing with AGO203, AGO206,

TABLE 2 Plasmids used in this study

Plasmid	Name	Vector	Relevant insert	Source or reference
None	pRS416			37
AGB005	pAGT141	pUC19	*GFP-GEN3*	38
AGB088	pAgShs1-GFP-Gen	pRS416	*SHS1-GFP-GEN3*	25
AGB123	pAgCdc12	pRS416	*CDC12*	19
AGB125	pAgCdc11	pRS416	*CDC11*	19
AGB127	pAgCdc3	pRS416	*CDC3*	19
AGB166	pAg Shs1	pRS416	*SHS1*	Peter Philippsen, University of Basel
AGB214	pAg Cdc11a-GFP-Gen	pRS416	*CDC11A-GFP-GEN3*	This study
AGB221	pAg Cdc3-GFP-Gen	pRS416	*CDC3-GFP-GEN3*	This study
AGB260	pAg Cdc12-GFP-Gen	pRS416	*CDC12-GFP-GEN3*	This study
AGB360	pAg Cdc11a S314A-GFP-Gen	pRS416	*CDC11A S314A-GFP-GEN3*	This study
AGB361	pAg Cdc12 S5A S8A-GFP-Gen	pRS416	*CDC12 S5A S8A-GFP-GEN3*	This study
AGB362	Cdc3 S91D-GFP-Gen	pRS416	*CDC3 S91D-GFP-GEN3*	This study
AGB371	Cdc12 S5E S8E-GFP-Gen	pRS416	*CDC12 S5E S8E-GFP-GEN3*	This study
AGB378	pAg Shs1 9D-GFP-Gen	pRS416	*SHS1 9D-GFP-GEN3*	25
AGB380	pAg Cdc3-GFP-Gen reduced	pRS416	*CDC3-GFP-GEN3*	This study
AGB383	pAg Cdc3 S91A-GFP-Gen	pRS416	*CDC3 S91A-GFP-GEN3*	This study
AGB384	pAg Cdc3 S496D-GFP-Gen	pRS416	*CDC3 S496A-GFP-GEN3*	This study
AGB385	pAg Cdc12 S323A-GFP-Gen	pRS416	*CDC12 S323A-GFP-GEN3*	This study
AGB386	pAg Cdc11a S314D-GFP-Gen	pRS416	*CDC11A S314D-GFP-GEN3*	This study
AGB425	pAg Shs1ΔCC-Cdc11a CC-GFP-Gen	pRS416	*SHS1ΔCC-CDC11A CC-GFP-GEN3*	This study
AGB470	pAg Cdc12 S5D-GFP-Gen	pRS415	*CDC12 S5D-GFP-GEN3*	This study

TABLE 3 Oligonucleotides used in this study

Oligonucleotide	Name	Sequence (5′–3′)
AGO5	Green2.2	TGTAGTTCCCGTCATCTTTG
AGO36	VG5	GGAGGTAGTTTGCTGATTGG
AGO98	New GEN3.3	CTTGCCATCCTATGGAACTG
AGO101	Cdc3 ORF seq 700F	TAGCGATCACAGGGATCAAG
AGO119	Cdc12 50R seq	TGCGATCTGCTGTAAACC
AGO130	Cdc11A ORF seq 700F	GTACTTGCGCTCGCTACTTC
AGO136	pET seq 1068 F	CCCAGCAAGGAAACTATC
AGO199	5′ 3CFP seq1	AGCATCTCCACGAGGCCAAG
AGO202	3′ 3CFP seq2	GTCTTGTAGTTCCCGTCATC
AGO203	5′ 11A RFP seq1	ACATACTTGGCACGGGAAGAG
AGO209	3 12 YFP seq1	TAACTCGGCGGCTGCAGAAG
AGO315	3′ CDC3-CFP:nat V	CTTGGCACACGCTGCTAAAG
AGO350	Ag CDC11A-Cherry iv	TACCAGCACCAGCATTCTC
AGO354	3′b Sep7-CFP 25ds	CCCTCGGGCAAAGGATAAGATATATAGTTAGAAGATGTTTGCCCATGATTACGCCAAGCTTGC
AGO405	5′ TUB4-CFP seq2	TTACTCACCACTGCGATCCC
AGO407	3′ TUB4-CFP seq2	ACCGGATTCAGTCGTCACTC
AGO427	Sep7V2	GCGCCCACAGTAGTGGTTTCAGA
AGO428	Sep7IV1	GCGGCTCTCAGGATAGGACGAA
AGO471	5′ kanR seq	TTACTCACCACTGCGATCCC
AGO472	kanR seqR	GGATCGCAGTGGTGAGTAAC
AGO520	GFP seq R	CGAGATTCCCGGGTAATAAC
AGO521	Gen seq F	TGGTGTCGCTCCTTCTAGTG
AGO534	conGFP I	AACCTTCGGGCATGGCACTC
AGO539	Cdc10 v2	CTGCAGGCATGCAAGCTTAG
AGO912	TubI seq F	AGACCACATGGTCCTTCTTG
AGO924	Cdc12 S5A S8A F	GAAATGTTGAATAGAGCGGATGGGGCCCTTGTTGGTATTTCTAAC
AGO925	Cdc12 S5A S8A R	GTTAGAAATACCAACAAGGGCCCCATCCGCTCTATTCAACATTTC
AGO926	Cdc12 S5E S8E F	GTTGAATAGAGAGGATGGGGAACTAGTTGGTATTTCTAACTTGCCAAACCAGCGG
AGO927	Cdc12 S5E S8E R	CCGCTGGTTTGGCAAGTTAGAAATACCAACTAGTTCCCCATCCTCTCTATTCAAC
AGO928	Cdc12 S5D F	CTTCAATTCAGGAGAAATGTTGAATAGAGACGATGGGTCACTTGTTGG
AGO950	Cdc12 S5D R	CTTCAATTCAGGAGAAATGTTGAATAGAGACGATGGGTCACTTGTTGG
AGO936	Cdc11a S314A F	CAAAGCTCATGAACAATGGGGCTACGGAATTTATCAGCTCACCAGCTC
AGO937	Cdc11a S314A R	GAGCTGGTGAGCTGATAAATTCCGTAGCCCCATTGTTCATGAGCTTTG
AGO938	Cdc11a S314D F	CAAAGCTCATGAACAATGGGGATACGGAATTTATCAGCTCACCAG
AGO939	Cdc11a S314D R	CTGGTGAGCTGATAAATTCCGTATCCCCATTGTTCATGAGCTTTG
AGO940	Cdc3 S91A F	CATCCACCGCAAGATCGCAGGATACGTGGGGTTCGCAAACC
AGO941	Cdc3 S91A R	GGTTTGCGAACCCCACGTATCCTGCGATCTTGCGGTGGATG
AGO942	Cdc3 S91D F	CCACCGCAAGATCGACGGATACGTGGGGTTCGCAAACC
AGO943	Cdc3 S91D R	GGTTTGCGAACCCCACGTATCCGTCGATCTTGCGGTGG
AGO946	Cdc3 S496D F	GGCGAACCAGAGTTCTCAGGATCCTGCACAGCCAAAGAAG
AGO947	Cdc3 S496D R	CTTCTTTGGCTGTGCAGGATCCTGAGAACTCTGGTTCGCC
AGO954	Cdc3 upstream seq F	ACATGCAGGCGTGGTCTTAG
AGO955	Cdc12 upstream seq F	AAGCGGATGGCAAAGGACTC
AGO982	Cdc12 S323A F	CTGCCCCAGCAAGGAAGCTAGCTCACAATCCAAAATTTAAGGAGG
AGO983	Cdc12 S323A R	CCTCCTTAAATTTTGGATTGTGAGCTAGCTTCCTTGCTGGGGCAG
AGO1065	Cdc11aΔCC F	CGGGAAGAGCAGATCAGGCTAGAGGAAAAGAGATTGAAGGCATTTAAAACGACGGCCAGTGAATTCG
AGO1066	Cdc11aΔCC R	CTCGAGGAATCGCTGTCCCTCTCGCTGCTTGCATGTGGTATTATCCATGATTACGCCAAGCTTGC
AGO1067	Cdc12ΔCC F	GAAGTACTTTACTGACCAGGTGAAGGCGGAAGAGCAGCGTTTCAGAAAAACGACGGCCAGTGAATTCG
AGO1068	Cdc12ΔCC R	GCCGGGCGGTAGAATCTTCTTGCTGATCTGTCATTTCTAGTTGGCATGATTACGCCAAGCTTGC
AGO1146	Cdc12 DS V	CCGCTTTCCGACAATACCTG
AGO1167	Shs1 Iseq F	GTACCAAACTCGGATGTACC

AGO471, AGO472, AGO521, and AGO539. The gel purified 4,504-bp product of AGB214 digested with BlpI and NheI was transformed into ΔlΔt to obtain strain AG384.1, which was verified by PCR using the oligonucleotides AGO98, AGO203, AGO405, and AGO350. AGB386 was obtained by using the primer pair AGO938/AGO939 on AGB214, digest verified using BciVI, and sequence verified using AGO130. AGB386 was transformed into ΔlΔt to obtain AG533.1. AGB360 was made using primer pair AGO936/AGO937 on ABG214, digest verified using BspHI, and sequence verified using AGO130. AGB360 was digested with XhoI and transformed into ΔlΔt to obtain AG669.2, which was verified by PCR using the primer pairs AGO5/AGO203, AGO471/AGO350, and AGO203/AGO350.

(iii) Cdc12 point mutation strain construction. AGB260 was made by cotransforming yeast with *GFP-GEN3* amplified from AGB141 by using the primer pair AGO218/AGO197 with AGB123. The plasmid was verified with XmaI, followed by sequencing with AGO136, AGO472, AGO520, and AGO521. The gel-purified 4,274-bp product of AGB260 digested with XhoI was transformed into ΔlΔt to obtain strain AG436.1,

which was verified by PCR using the oligonucleotides AGO119, AGO202, AGO209, and AGO407. AGB361 was made by using the primer pair AGO924/AGO925 on AGB260, digest verified using ApaI, and sequence verified using AGO955. AGB361 was digested with BciVI and PacI and transformed into ΔlΔt to obtain AG671.1, which was verified by PCR with primer pairs AGO955/AGO101 (followed by digestion with ApaI to verify point mutation), AGO203/AGO5, AGO471/AGO119, and AGO209/AGO119. AGB385 was obtained by using the primer pairs AGO982/AGO983 on AGB260, digest verified using NheI, and sequence verified using AGO5 and AGO954. AGB385 was digested using ApaI and BciVI and transformed into ΔlΔt to obtain AG672, which was verified using primer pairs AGO203/AGO5, AGO471/AGO119, and AGO209/AGO119. AGB470 was obtained using the primer pairs AGO928/929 on AGB260 and sequence verified using AGO5 and AGO954. AGB470 was transformed into ΔlΔt to obtain strain AG674. AGB371 was obtained using the primer pairs AGO926/AGO927, digest verified using SpeI, and sequence verified by using AGO5 and AGO955.

AG537.1 was obtained by transforming AGB378 into ΔlΔt. AG652.1 was made by transforming ΔlΔt with a gel-purified 2,901-bp product amplified off BglI/PciI-digested AGB005 template DNA by using the primer pair AGO1067/AGO1068. Heterokaryons were verified by using the primers AGO136, AGO405, AGO471, and AGO1146. AG656.1 was obtained by transforming ΔlΔt with a gel-purified 2,901-bp product amplified off BglI/PciI-digested AGB005 template DNA by using the primer pair AGO1065/AGO1066. Heterokaryons were verified by using the primers AGO130, AGO350, AGO405, and AGO407. Strain construction for AG657.1 was as follows: AGB214 was digested with AflII/BlpI, and the 3,887-bp band was gel purified and used as a Cdc11a-GFP-Gen PCR template. The PCR product was amplified by using AGO1140/AGO354, and the resulting product was cotransformed in yeast with AGB166 to yield AGB425. The plasmid was digest verified with BlpI/BsrGI and sequence verified using AGO36, AGO98, AGO427, AGO428, AGO472, AGO521, AGO534, and AGO912. AGB425 was digested with BlpI/PciI, and the 5,096-bp digestion product was gel extracted and transformed into ΔlΔt to obtain AG657.1. Heterokaryons were verified by PCR using the primers AGO98, AGO427, AGO534, and AGO1167.

PCR was performed according to standard methods with polymerases from Roche Diagnostics (Indianapolis, IN) and New England BioLabs (Beverly, MA). Oligonucleotides were synthesized by Integrated DNA Technologies (Coralville, IA), and all restriction enzymes were obtained from New England BioLabs. Plasmid isolation from yeast and sequencing were performed as previously described (50). All sequencing was performed by Dartmouth College Core Facilities (Hanover, NH). Radial growth assays were performed as previously described (39).

Microscope setup and image processing. A Zeiss Axioimage-M1 upright light microscope (Carl Zeiss, Jena, Germany) equipped with a Plan-Apochromat ×63/1.4NA oil objective lens was used for wide-field fluorescence microscopy and a Plan-Neofluar ×100/1.3 NA oil objective was used for phase-contrast imaging of spores. The green fluorescent protein (GFP) signal was visualized with a Zeiss 38HE filter set and Alexa Fluor 568 signal was visualized with Chroma filter set 41002B. An Exfo X-Cite 120 lamp was used as the fluorescent light source. Images were acquired on an Orca-AG charge-coupled device camera (C4742-80-12AG; Hamamatsu, Bridgewater, NJ) driven by Volocity 5 (Perkin-Elmer, Waltham, MA). Live and immunofluorescence images were taken at 0.5-μm steps to encompass the depth of the entire hypha and fast deconvolved in Volocity 4. For live images used to ascertain the fluorescence intensity of a given area, 0.5-μm steps were taken over a total thickness of 9 μm.

Confocal time-lapse movies were acquired using a Yokogawa spinning disk attached to a Nikon (Melville, NY) Eclipse Ti utilizing a Nikon ×100 1.4NA Plan Apo VC objective lens, controlled by MetaMorph 7 (Molecular Devices, Sunnyvale, CA). This system was assembled by Quorum Technologies (Guelph, Ontario, Canada). Photobleaching of entire septin rings was performed using a 405 nm laser at 70% power (1,000 ms, 450 mW laser) in conjunction with a Mosaic micro-mirror array system. Images were captured using a Hamamatsu ImagEM C9100-13 EM-CCD camera. GFP was imaged using 30% laser power (491 nm laser) exposed for 250 ms/slice. Seventeen-slice *z*-stacks (0.5-μm steps) through the entire hypha were imaged at 30-s intervals.

Live *Ashbya* cells were imaged on 2% agarose gel pads made with ×2 low-fluorescence minimal media, covered with a glass coverslip, and sealed with VALAP. All images presented here are maximum projections of three-dimensional volumes.

TABLE 4 Shs1 IR rings FRAP statistics

Strain	*n*	Mean ± SD[a]	
		Mobile fraction (%)	$t_{1/2}$ (s)
Shs1-GFP (AG442.1)	7	25.3 ± 4.9	54.7 ± 8.5
Shs1-GFP 9D (AG537.1)	7	37.8 ± 11.1*	38.8 ± 13.9*

[a] *, $P < 0.05$ (two-tailed *t* test).

Fluorescence intensity and FRAP analysis. Fluorescence intensity measurements were taken in Volocity 4 and FRAP (fluorescence recovery after photobleaching) measurements were taken in Volocity 5. Mean fluorescence intensity measurements for septin rings and septin clouds at hyphal tips were measured using a region of interest of the same area for each structure type. Cytosolic background was measured by subtracting an average of five background mean fluorescence measurements in the same cell as the measured ring from the mean fluorescence intensity of the ring.

To measure the intensity of a given ring over the course of a FRAP movie, a region of interest was drawn around the entire ring, and the mean fluorescence value per pixel of the selected area was recorded. An adjacent region of cytosol was measured, and this mean fluorescence value was subtracted from the mean fluorescence of the ring to yield the mean fluorescence of the ring minus the background. Photobleaching was corrected for using the mean fluorescence intensity of a ring of the same type in the same field. The regions of interest around the rings were shifted if necessary to compensate for cell drift during the movie. The mobile fractions for each ring were calculated by dividing the percent recovery by the percent bleach, and mobile fractions were averaged to obtain the average mobile fractions and standard deviations listed in Table 4. The $t_{1/2}$ for each ring was calculated using the formula $t_{1/2} = t_{maxfl} \cdot [\log(0.5)/\log(1/\text{mobile fraction})]$, where t_{maxfl} is the time point where recovery plateaus. The average $t_{1/2}$ and standard deviation values are listed in Table 4. The statistical significance of the mobile fraction and $t_{1/2}$ measurements were determined by two-tailed *t* tests.

Immunofluorescence. Immunofluorescence was performed as described previously (40). Rabbit anti-ScCdc11p (Santa Cruz Biotechnology, Santa Cruz, CA) or Rabbit anti-GFP (Invitrogen) was diluted in 1× phosphate-buffered saline plus 1 mg of bovine serum albumin/ml and used at a 1/100 dilution. Cells were incubated with primary antibody overnight at 4°C. Primary antibody was detected and visualized using Alexa Fluor 488-labeled anti-rabbit antibody (Invitrogen) at a 1/200 dilution.

Protein extraction and purification. Cells were grown in *Ashbya* full media (AFM) for 16 h and harvested by vacuum filtration. For lysis, 500 mg of cells was resuspended in 1 ml of ice-cold lysis buffer (50 mM HEPES-KOH [pH 7.6], 1 M KCl, 1 mM $MgCl_2$, 1 mM EGTA, 5% glycerol, 0.45% Tween 20, 2× protease inhibitor cocktail). For lysates used to analyze the phosphorylation status of the septin complex by mass spectrometry, phosphatase inhibitors (50 mM NaF and 100 mM β-glycerophosphate) were added to the lysis buffer. Cells were lysed by bead beating with 0.5-mm zirconia/silica beads in a MiniBeadbeater-8 (BioSpec Products, Bartlesville, OK) at top speed for five intervals of 90 s with 30-s rest. Cell lysates were clarified by centrifugation for 10 min at 16,100 × *g*. Protein concentrations were determined by using the Bradford assay.

Septin complexes to be analyzed by mass spectrometry were purified from AG495.1 (Cdc11-TAP) lysates using rabbit IgG (Millipore, Billerica,

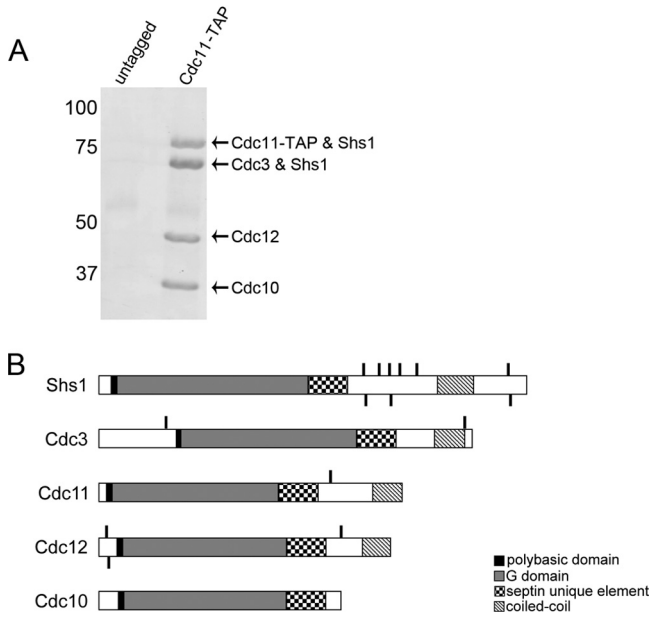

FIG 1 *Ashbya* septins are phosphorylated. (A) Four of the five septins in *Ashbya* are phosphorylated. The septin complex was immunoprecipitated from *Ashbya* lysates (AG495.1). Proteins were separated by SDS-PAGE and stained with Coomassie blue. All four bands (representing five septins) were excised from the gel and submitted for mass spectrometry analysis, revealing that four of the five septins are phosphorylated. Mass spectrometry peptide coverage was as follows: Cdc3, 77%; Cdc10, 79%; Cdc11, 67%; Cdc12, 92%; and Shs1, 70%. (B) Schematics outlining phosphorylation sites and conserved domains of the *Ashbya* septins. Phosphorylation sites are indicated as black lines on the schematic.

MA) bound to Dynabeads (Invitrogen) according to the manufacturer's instructions. Lysates containing 15 mg of total protein were incubated with 100 μl of IgG-coupled Dynabeads for 3 h at 4°C. Beads with precipitated proteins were separated from lysates on a magnet and washed five times with 3 ml of immunoprecipitation wash buffer (100 mM HEPES-KOH pH 8.0, 200 mM magnesium acetate, 1 mM $MgCl_2$, 300 mM sodium acetate, 10 mM EGTA, 0.1 mM EGTA, 10% glycerol, 0.5% NP-40). Precipitated proteins were eluted in 25 μl of 1× sample buffer, reduced with β-mercaptoethanol, and separated on a 10% acrylamide gel (16 by 18 cm) by SDS-PAGE at 25 mA for 7 h. The proteins were stained using the colloidal blue staining kit (Invitrogen). Four bands representing all five septins were excised and analyzed for phosphorylation, acetylation, and SUMOylation by the Taplin Biological Mass Spectrometry facility (Harvard Medical School, Boston, MA). Mass spectrometry peptide coverage was as follows: Cdc3, 77%; Cdc10, 79%; Cdc11, 67%; Cdc12, 92%; and Shs1, 70%.

Western blotting. Western blotting was performed by standard methods as previously described (25). Membranes were probed with rabbit polyclonal anti-GFP antibody (ab290; Abcam, Cambridge, MA) and rat monoclonal anti-α-tubulin antibody (AbD Serotec, Raleigh, NC), both at a 1:1,000 dilution. Densitometry analysis to determine relative abundance of proteins was done in ImageJ (National Institutes of Health, Bethesda, MD) using the gel analysis tools.

RESULTS

***Ashbya* septins are phosphorylated.** We hypothesized that septins in *Ashbya* are phosphorylated, based on previous data revealing that the kinases Elm1p and Gin4p lead to a loss of septin structure formation (19). To identify phosphorylation sites, we first immunoprecipitated TAP-tagged Cdc11p in order to pull out the entire septin complex and assessed the coprecipitating proteins by SDS-PAGE (Fig. 1A). The five constituents of the septin complex resolve as four bands, due to the comigration of high-molecular-weight Shs1 with Cdc11-TAP and low-molecular-weight Shs1 with Cdc3 (Fig. 1A). All four bands were excised from the gel and submitted for mass spectrometry analysis. Although we analyzed the proteins for several posttranslational modifications—phosphorylation, acetylation, and SUMOylation—the only modification identified on any of the septins was phosphorylation. We previously reported Shs1p is multiphosphorylated at nine sites (25) and show here that three of the remaining four septins are also phosphorylated (Fig. 1B and Table 5). The majority of these sites are novel, that is, they are not conserved on the primary sequence level with phosphorylation sites previously identified in the septins of *S. cerevisiae* and *C. albicans* (see Fig. S1 in the supplemental material) (23). Many of the *Ashbya* septin phosphorylation sites are found in proximity to septin polybasic and coiled-coil domains, which are thought to be important in septin interactions with membranes and with one another. We set out to examine whether phosphorylation of these sites influences the assembly of septins into higher-order structures.

Mutation of septin phosphorylation sites affects cell and septin morphology. In order to assess the function of septin phosphorylation, we made phosphomimetic (site changed to aspartic acid or glutamic acid) and nonphosphorylatable (site changed to alanine) point mutations to the identified phosphorylation sites of GFP-tagged septins. These mutants were tested for their effects on cell and septin morphology. Some of the mutations caused no obvious cell or septin phenotypes (Table 6). Representative images of normal-looking septin structures at the interregion, branch sites, and at hyphal tips are shown for nonphosphorylatable Cdc12 S5A S8A and Cdc12 S323A mutants in Fig. 2A. The normal cell growth and septin structure formation in these mutants indicate that a subset of septin phosphorylation sites are dispensable for normal cell growth and assembly of higher-order septin structures. Other alterations to phosphorylation sites did lead to obvious cell and septin phenotypes. The nonphosphorylatable mutant Cdc11 S314A and the phosphomimetic mutant Cdc3 S91D led to production of abnormally shaped ascospores. Wild-type ascospores are straight and needle-like, however both the Cdc11 S314A and Cdc3 S91D mutations resulted in spores that were curved and crescent-shaped (Fig. 2B). Despite their unusual shape, the crescent-shaped ascospores were not detectably defective in germination. This alteration in spore shape also did not lead to any significant change in cell growth, based on radial growth of cells on agar plates over the course of 10 days (Fig. 2C), indicating that spore shape does not impact mycelial growth rates. Intriguingly, when Cdc11 S314A and Cdc3 S91D mutant cells were assessed for their ability to form higher-order septin structures, we found that the mutant septins were not localizing to any

TABLE 5 Septin phosphorylation sites identified by mass spectrometry

Septin	Phosphorylation site(s)
Cdc11	S314
Cdc12	S5, S8, S323
Cdc3	S91, S496
Cdc10	No sites identified
Shs1	S359, S362, S380, T394, S396, S408, S431, T555, S558

TABLE 6 Summary of phosphorylation site mutation phenotypes

Phosphorylation site mutation[a]	Ashbya strain no.	Phenotype
Cdc11 S314A	AG669.2	Sickle-shaped spores
Cdc11 S314D*	AG533.1	None observed
Cdc12 S5A S8A	AG671.1	None observed
Cdc12 S5E S8E*	—	Dominant lethal
Cdc12 S5D*	AG674	None observed
Cdc12 S323A	AG672	None observed
Cdc3 S91A*	AG529.1	None observed
Cdc3 S91D	AG668.1	Sickle-shaped spores
Cdc3 S496D*	AG531.1	None observed
Shs1 9A	AG643.1	No immediately obvious cell, spore, or septin ring phenotypes were observed. However, further investigation revealed an increase in steady-state localization to septin rings and a trend toward decreased mobility observed by FRAP[b]
Shs1 9D	—	Recessive lethal
Shs1 9D*	AG537.1	Increased dynamics at IR rings

[a] All mutants were scored for cell, spore, and septin ring morphological defects. Mutations indicated by asterisks (*) were introduced on a plasmid, while the remainder were integrated at the endogenous locus. All were tagged with GFP to observe localization to septin structures.
[b] Meseroll et al. (25).

higher-order structure (Fig. 2D). Remarkably, when the opposite mutant (i.e., Cdc11 S314D and Cdc3 S91A) for each of these was tested, we found that neither had any impact on cell or septin morphology (Table 6). This indicates that specific changes in phosphorylation status of individual septin phosphorylation sites can have severe functional consequences.

Phosphomimetic mutant Cdc12 S5E S8E is dominant lethal. Although the majority of mutants we tested did not affect cell health, some mutants had extremely deleterious effects on cell viability. The phosphomimetic mutant Cdc12 S5E S8E was lethal to *Ashbya* cells even when introduced on a plasmid in the presence of the wild-type genomic Cdc12 (Table 6). Attempts to heterologously express this mutant on a plasmid in the budding yeast *Saccharomyces cerevisiae* also resulted in a lethal phenotype. Due to its dominant lethal effects, we were unable to assess the precise role of Cdc12 S5E S8E in septin organization. The single phosphomimetic mutant Cdc12 S5D expressed on a plasmid in *Ashbya* displayed normal cell and septin morphology (Table 6), indicating that the deleterious effects of Cdc12 S5E S8E are due either to the double mutant or S8E alone. Thus, we have identified Cdc12 S5E S8E, as a novel dominant-negative septin allele.

Phosphomimetic Shs1p has increased dynamics at IR rings. In several systems, phosphorylation of septins has been shown to modulate septin dynamics (24, 25, 41, 42). Shs1p is by far the most heavily phosphorylated septin in *S. cerevisiae* and *A. gossypii* (22, 25); thus, we have focused extensive effort on analysis of the regions containing and residing near the Shs1p phosphorylation sites. We previously reported that when all nine phosphorylation sites on Shs1p have been mutated to phosphomimetic aspartic acid (Shs1 9 × S/T 359-558 D, hereafter called Shs1 9D) and the mutant allele is expressed as the only copy of *SHS1* at its endogenous locus, the result is cell lethality as germlings with germ bubbles and, infrequently, small germ tubes (25). Unlike Cdc12 S5E S8E, however, the lethality of phosphomimetic Shs1 9D is recessive, and cells expressing the mutant on a plasmid in addition to a wild-type copy of *SHS1* are healthy. Shs1 9D-GFP localizes normally to higher-order septin rings and tip structures (Fig. 3A). Because we know from previous work (25) that the nonphosphorylatable Shs1 9A-GFP mutant protein is more concentrated at interregion (IR) rings than its wild-type counterpart Shs1-GFP, we hypothesized that, although Shs1 9D-GFP localizes to septin structures, the phosphomimetic mutant protein concentration at these structures is altered from wild-type levels. To test this, we measured the fluorescence intensity of Shs1 9D-GFP and Shs1-GFP in a region of fixed size for the IR rings ($n \geq 16$ each strain), branch rings ($n \geq 17$ each strain), and tips ($n \geq 15$ each strain). We found that there was no significant difference in fluorescence intensity between Shs1 9D-GFP and Shs1-GFP in any of the septin structures (Fig. 3B), indicating that steady-state concentration of the mutant is comparable to the wild type. Although the steady-state levels of the mutant are not different from the wild type, we considered that Shs1 9D dynamics may differ from those of Shs1. We tested this possibility by performing FRAP on Shs1-GFP or Shs1 9D-GFP at the IR rings ($n = 7$ rings each). These FRAP experiments revealed that Shs1 9D-GFP has a statistically significantly increased mobile fraction and statistically significantly decreased $t_{1/2}$ at the IR rings compared to wild-type Shs1-GFP (Fig. 3C and Table 4, $P < 0.05$ for both mobile fraction and $t_{1/2}$). Thus, although the steady-state fluorescence intensities are similar for the mutant compared to the wild type, Shs1 9D-GFP is more dynamic, i.e., a greater percentage of Shs1 9D-GFP can recover more quickly than the wild type. It is unclear whether this change in dynamics could affect cell viability in the absence of any wild-type Shs1p, or if some other unidentified property of the phosphomimetic mutant is the culprit for the lethal phenotype.

Shs1p requires its specific coiled coil to incorporate into septin rings. Increased dynamics in mutant Shs1p is not without precedent. We demonstrated in previous work that deletion of the Shs1p coiled-coil domain leads to a greatly increased mobile fraction of Shs1 at IR rings without affecting the dynamics of other septins (25). The Shs1p coiled-coil deletion mutant also exhibits greatly expanded branch rings that extend beyond the boundaries of normal branch rings. We sought to determine whether these dynamics- and ring size-limiting properties were specific to the Shs1p coiled coil. To test this, we truncated Shs1p after residue 358, which phenocopies the deletion of the Shs1 coiled-coil domain alone for all features tested (25), replaced the deleted region with the predicted coiled-coil domain of Cdc11 (residues 371 to 411, Fig. 4A), and observed the effects on septin structure. Strikingly, the chimeric Shs1 (residues 1 to 358) with the Cdc11 coiled-coil domain (Shs1-Cdc11 CC-GFP) does not localize to any septin structures but is instead distributed throughout the cytoplasm of the cell (Fig. 4B). We hypothesized that the loss of Shs1p at the rings would lead to an inability of septin rings to form at all and were surprised to find that when Cdc11 is visualized via immunofluorescence in the Shs1-Cdc11 CC-GFP cells, we see it localizing to expanded branch ring structures that phenocopy those found in the Shs1p coiled-coil deletion cells (Fig. 4C). To exclude the possibility that the Shs1-Cdc11 CC-GFP construct is defective in GFP fluorescence and thus not able to be visualized in the septin assemblies, we confirmed its cytoplasmic localization using anti-GFP immunofluorescence (Fig. 4D). The expression levels of Shs1-Cdc11 CC-GFP were comparable to the wild type, as assessed by Western blotting (Fig. 4E), so the localization defect is not simply a result of misexpression of the chimeric protein. These data indicate that septin rings in *Ashbya* can form in the absence of Shs1p in the higher-order structure and that the introduction of the Cdc11 coiled coil to Shs1p inhibits the incorporation of Shs1p into higher-order septin structures. Furthermore, the expanded

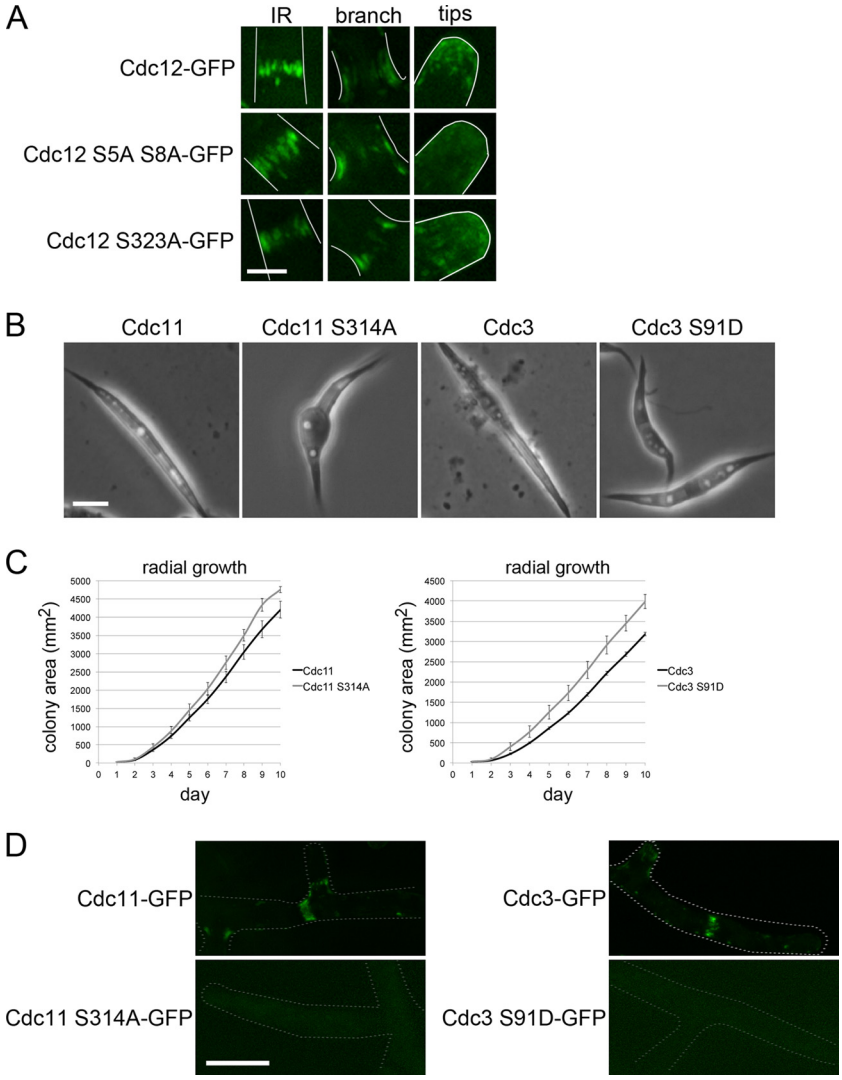

FIG 2 Some septin phosphorylation sites influence cell shape and viability, as well as septin morphology. (A) Representative images of septins in phosphorylation mutants that have no observed effect on cell or septin morphology. Cdc12-GFP (AG436.1), Cdc12 S5A S8A-GFP (AG671.1), and Cdc S323A-GFP (AG672) were visualized by wide-field fluorescence microscopy. Bar, 2.5 μm. (B) Ascospore shape is perturbed by mutations in septin phosphorylation sites. Ascospores produced by wild-type Cdc11-GFP (AG384.1) and Cdc3-GFP (AG413.2) and their respective phosphorylation mutant counterparts, Cdc11 S314A-GFP (AG669.2) and Cdc3 S91D-GFP (AG668.1), were imaged by phase-contrast microscopy. Bar, 5 μm. (C) Crescent-shaped spores have no significant effect on cell growth. Cdc11-GFP, Cdc11 S314A-GFP, Cdc3-GFP, and Cdc3 S91D-GFP cells were grown on AFM G418 agar plates for 10 days ($n = 3$ each strain). Plates were imaged every 24 h, and the colony growth area was measured. (D) Septin phosphorylation is required for normal septin morphology. Cdc11-GFP, Cdc11 S314A-GFP, Cdc3-GFP, and Cdc3 S91D-GFP were imaged by wide-field fluorescence microscopy. For both mutants, alteration of these phosphorylation sites leads to a loss of septin structures. Dotted white lines represent cell outlines. Bar, 10 μm.

septin structures observed in the mutant strain suggest that any loss of the Shs1p coiled coil, even if replaced with another septin's coiled coil, leads to aberrantly large septin rings.

We previously showed that loss of the Shs1 C terminus leads to more frequent lateral branches (25). In the Shs1-Cdc11 CC-GFP chimera, despite the loss of Shs1p at the ring, the distance between lateral branches is not significantly altered in the chimeric mutant compared to the wild type (19.8 ± 11.8 μm for wild type versus 19.1 ± 11.2 μm for the chimera, $n > 95$, $P > 0.6$ by two-tailed t test). These results suggest that the normal position and frequency of lateral branches is not dependent on the localization of Shs1p to the ring. Finally, this also suggests then that the increased branching frequency previously observed (25) does depend on the presence of the mutant Shs1 at the ring and is not simply the consequence of expanded ring zones.

Cdc11p and Cdc12p coiled coils are required for normal septin ring morphology. Based on the remarkable septin organization phenotypes we observed upon swapping the Shs1p coiled coil for that of Cdc11p, we hypothesized that the coiled-coil domains of other septins also impact septin ring morphology. We tested this by separately deleting the coiled coils of Cdc11p (residues 371 to 411) and Cdc12p (residues 352 to 390) (Fig. 5A). The loss of either coiled-coil domain led to major defects in septin higher-order structures. Cdc11ΔCC-GFP was observed to localize diffusely to the cytoplasm (Fig. 5B); however, the GFP signal is very dim, and when Cdc11ΔCC-GFP expression levels were assessed

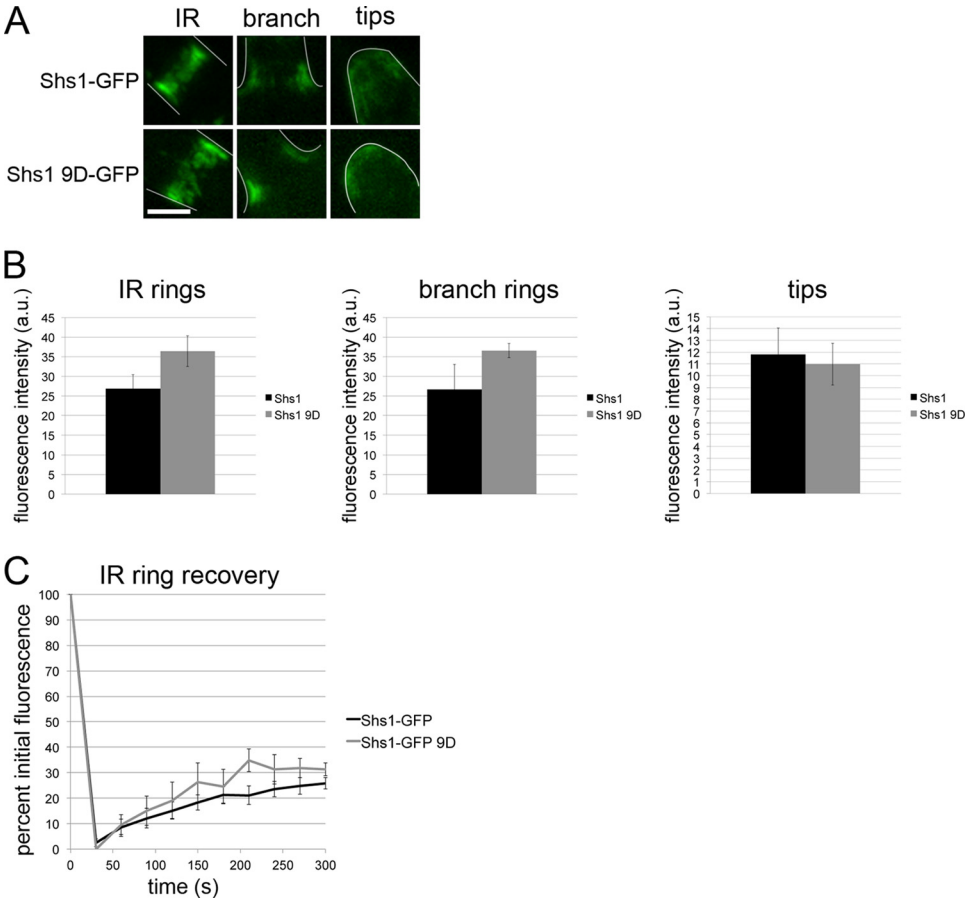

FIG 3 Phosphomimetic mutations in Shs1 increase septin dynamics. (A) Cells expressing Shs1-GFP (AG442.1) and Shs1 9D-GFP (AG537.1) from a plasmid were imaged by wide-field fluorescence microscopy. Despite the mutations, all septin structures are able to form in the Shs1 9D-GFP cells. White lines represent cell outlines. Bar, 2.5 μm. (B) Concentration of Shs1 9D-GFP in any septin structure does not significantly vary from its wild-type counterpart. Cells plasmidically expressing Shs1-GFP and Shs1 9D-GFP were imaged on a wide-field fluorescence microscope, and images were contrasted to the same levels. Fluorescence intensities for a given volume of individual rings and tips were measured ($n \geq 15$ for each structure in each strain). Cytoplasmic background was subtracted. Error bars represent the standard error. No statistically significant differences in the steady-state fluorescence intensity were observed for any structure. (C) Shs1 9D-GFP has increased dynamics at IR rings compared to wild-type Shs1-GFP. Cells plasmidically expressing Shs1-GFP and Shs1 9D-GFP were imaged by using confocal spinning disk microscopy. Individual IR rings in each strain were bleached and imaged every 30 s for 5 min ($n = 7$ rings per strain). The fluorescence intensity of the bleached region was recorded at each time point. Intensities were corrected for cytoplasmic background and photobleaching. Error bars on the recovery curves represent the standard error. The statistical significance for mobile fraction and $t_{1/2}$ were determined by two-tailed *t* tests (Table 4). The mobile fraction was significantly increased, and $t_{1/2}$ was significantly decreased for the mutant rings compared to the wild type.

by Western blotting, they appear to be much lower than wild-type Cdc11-GFP levels (Fig. 5C). Loss of the Cdc12p coiled coil leads to several cellular effects. Spore germination is greatly reduced in these cells; thus, obtaining a quantity of fully grown cells for this strain is challenging. Those that do grow demonstrate diverse septin phenotypes. In the majority of Cdc12ΔCC mutant cells (78%, $n = 27$ cells total), Cdc12ΔCC-GFP localizes diffusely to the cytoplasm (Fig. 5B, Cdc12ΔCC-GFP left-hand panel); however, in smaller percentages of cells, the protein localizes to cytoplasmic circles and crescents (15%, Fig. 5B, Cdc12ΔCC-GFP, middle panel) or septin rings (7%, Fig. 5B, Cdc12ΔCC-GFP, right-hand panel). Thus, in 93% of the cells observed, Cdc12ΔCC-GFP is unable to localize to septin rings. These data suggest that septin coiled-coil domains are able to perform different roles: the Shs1p coiled coil limits septin ring size, although the Cdc12p, and perhaps Cdc11p, coiled coils are required for septin higher-order structures to form at all.

DISCUSSION

We demonstrate in this study the novel and various effects of septin phosphorylation and coiled-coil domain mutations in *Ashbya*. Alteration to the status of septin phosphorylation sites leads to diverse phenotypes. Mutation of some phosphorylation sites have no apparent impact on cell or septin morphology, while others led to defects in cell and septin structure shape. The phosphomimetic mutants Cdc12 S5E S8E and Shs1 9D are so deleterious as to cause cell lethality. Similarly, we show here that septin coiled-coil domains also perform diverse functions. The Shs1p coiled-coil domain acts to limit septin ring size, while the Cdc12p and Cdc11p coiled-coil domains are required for the formation of septin rings. The variety of effects of septin phosphorylation sites and coiled-coil domains suggests that septins can be regulated in many different ways to achieve the functions they perform in the cell. Importantly, phosphorylation does not provide a generic

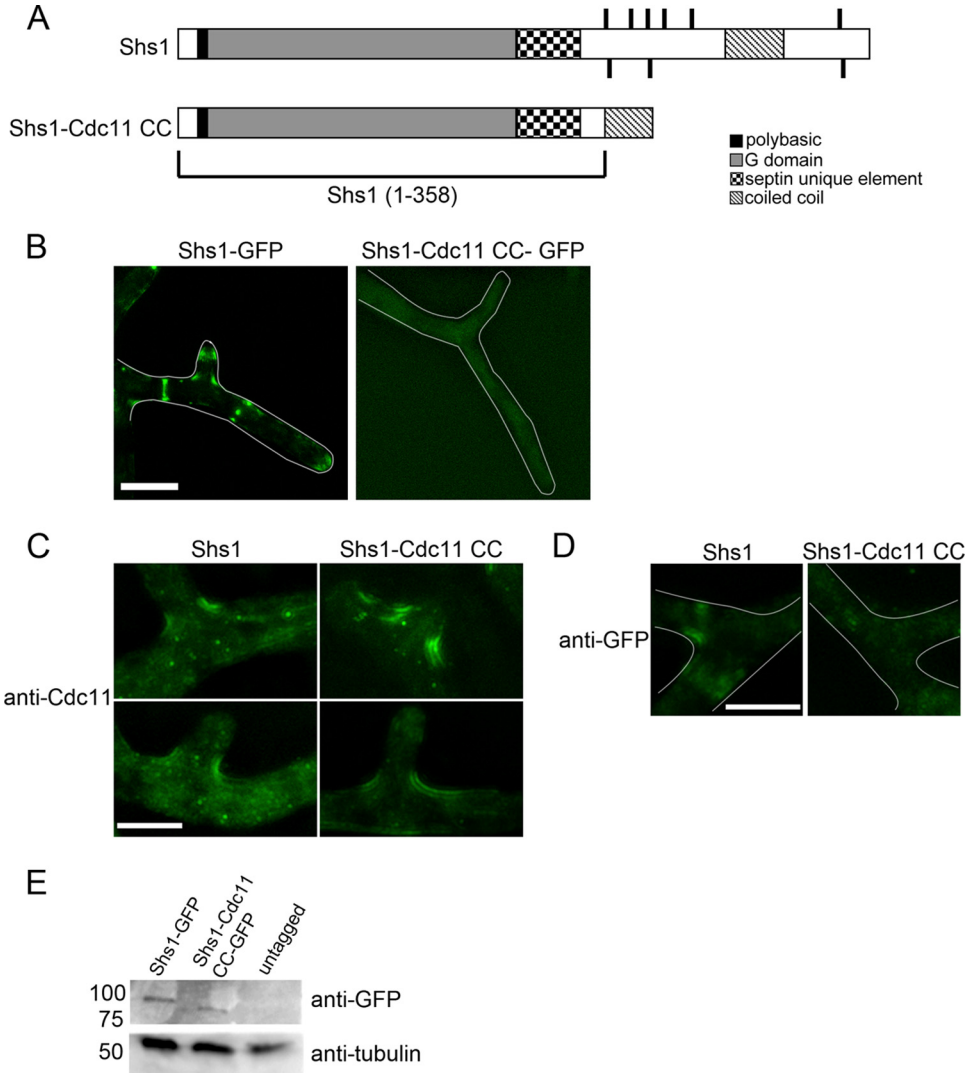

FIG 4 Shs1 requires its specific coiled coil to incorporate into septin rings. (A) Schematic representation of the Shs1-Cdc11 CC chimera. A C-terminally truncated Shs1 (residues 1 to 358) was appended with the Cdc11 coiled coil (residues 371 to 411). Phosphorylation sites are indicated as black lines on the schematic. (B) Shs1-GFP (AG124) and Shs1-Cdc11 CC-GFP (AG657.1) were imaged by wide-field fluorescence microscopy. The chimeric Shs1 with the Cdc11 coiled coil localizes diffusely to the cytoplasm but does not incorporate in septin structures. White lines represent cell outlines. Bar, 10 μm. (C) Anti-Cdc11 immunofluorescence was performed on Shs1-GFP and Shs1-Cdc11 CC-GFP cells. Cdc11 localizes to expanded septin structures at branch sites in the chimeric mutant cells. Bar, 5 μm. (D) Anti-GFP immunofluorescence was performed on Shs1-GFP and Shs1-Cdc11 CC-GFP cells. Shs1 localizes to septin structures in wild-type cells but only diffusely localizes to the cytoplasm in the coiled-coil swap mutant. Bar, 5 μm. (E) The expression levels of the chimeric Shs1 are comparable to the wild type. *Ashbya* lysates for the indicated strains grown at 37°C were separated on SDS-PAGE (10% acrylamide) and probed with anti-GFP and anti-α-tubulin antibodies. The relative abundances of the wild-type and chimeric proteins were 1.00 and 0.92, respectively, as determined by densitometry analysis on the blot.

switch but rather can promote or limit organization depending on the subunit context.

The variability in the impact of *Ashbya* septin phosphorylation is intriguing. Studies focusing on the roles of septin phosphorylation in other organisms such as the budding yeast *Saccharomyces cerevisiae* and the fungus *Candida albicans* have revealed that prevention of septin phosphorylation affects cell and septin morphology (22, 28). Mutations made to *S. cerevisiae* Shs1p phosphorylation sites result in mutant cells that are larger and have aberrant cell morphology (22). *C. albicans* Cdc11p phosphorylation is required for cells to transition to hyphal growth but did not impact septin localization (28). Loss of the Gin4p kinase, which has been shown to direct phosphorylate Shs1p in *S. cerevisiae* and *C. albicans*, impairs septin ring formation and dynamics (24, 27, 28, 43, 44). Although we have yet to identify whether any septins are the target of the Gin4p and Elm1p kinases in *Ashbya*, deletion of either of these kinases leads to an inability of IR rings to assemble (19). We show here that mutations to individual sites in the septins Cdc3p and Cdc11p causes *Ashbya* to produce misshapen ascospores and prevents either of the mutant proteins from localizing to septin structures. It is interesting that the mutation to Cdc3 is phosphomimetic (S91D), whereas the Cdc11 mutation is nonphosphorylatable (S314A). This suggests that, depending upon the context, inhibition of phosphorylation and dephosphoryla-

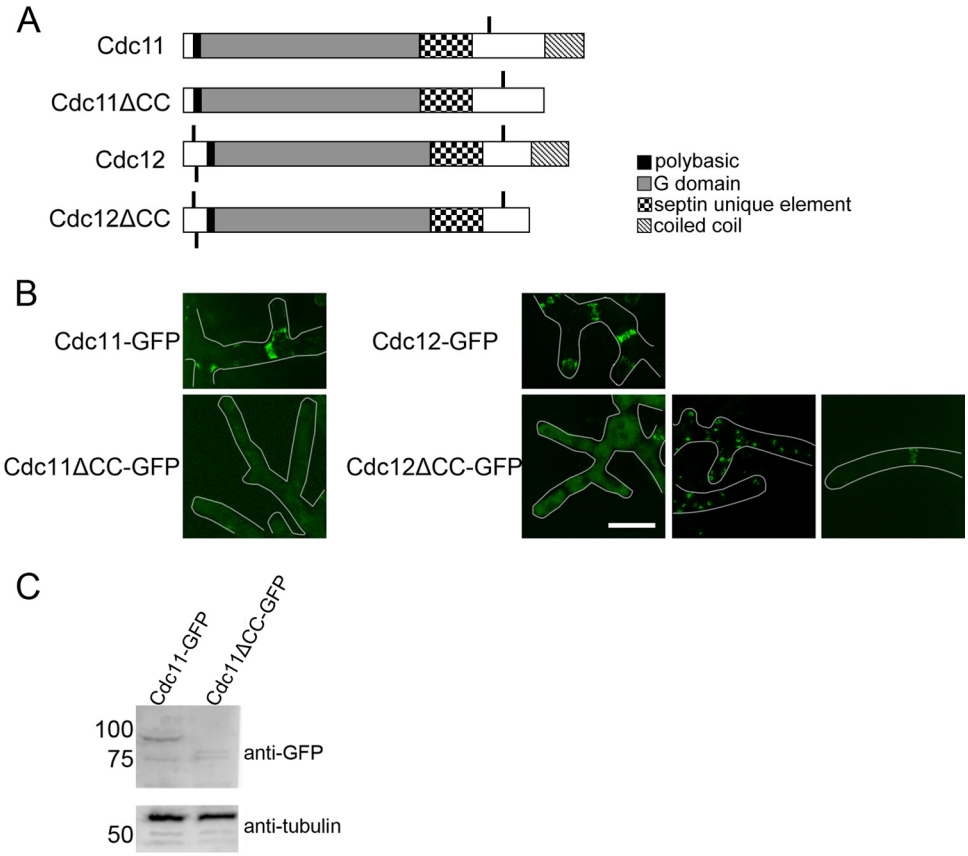

FIG 5 Cdc11 and Cdc12 coiled coils are essential for normal septin morphology. (A) Schematic representation of Cdc11 and Cdc12 coiled-coil deletion mutant proteins. The predicted coiled-coil domains of Cdc11 (residues 371 to 411) and Cdc12 (residues 352 to 390) were deleted. Phosphorylation sites are indicated as black lines on the schematic. (B) Cdc11-GFP (AG384.1), Cdc11ΔCC-GFP (AG656.1), Cdc12-GFP (AG436), and Cdc12ΔCC-GFP (AG652.1) were imaged by wide-field fluorescence microscopy. Loss of either the Cdc11 or Cdc12 coiled-coil domain leads to defects in septin ring morphology. White lines represent cell outlines. Bar, 10 μm. (C) Expression levels of Cdc11-GFP are decreased in the Cdc11 coiled-coil deletion strain. *Ashbya* lysates for the indicated strains grown at 37°C were separated on SDS-PAGE (10% acrylamide) and probed with anti-GFP and anti-α-tubulin antibodies. Cdc11-GFP migrates at ~90 kDa and Cdc11ΔCC-GFP migrates at ~75 kDa.

tion of the septins can have similar effects. Remarkably, if the opposite mutation is made to these phosphorylation sites (i.e., Cdc3 S91A or Cdc11 S314D), we see no apparent cell or septin phenotypes. While it is unclear why these particular sites may be important, we speculate that the nearness of the Cdc3 S91 site to this septin's polybasic region (Fig. 1B) may enable phosphorylation to regulate the exposure of this region and help direct its interaction with the membrane. Although S314 is not particularly near to any of Cdc11's conserved domains, it was the only site we identified for Cdc11, and its phosphorylation clearly plays some important functional role in cell morphology and septin structure formation. Future work with these mutants will be required to parse out the mechanism of these sites' functionalities.

In addition to the cell and septin phenotypes we observed with the aforementioned Cdc11 and Cdc3 mutants, we identified some septin phosphorylation sites to be even more crucial to cell health. The phosphomimetic double point mutant Cdc12 S5E S8E was dominant lethal and phosphomimetic mutations to all nine Shs1p phosphorylation sites led to cell lethality if expressed as the only copy of *SHS1* in the cell. The severity of these phosphorylation mutant phenotypes is unprecedented in the septin field, and we aim to uncover a mechanism for the lethality in the future.

The effects of Cdc12 S5E S8E may also be explained by the nearness of these sites to the polybasic domain of Cdc12. It is possible that the negative charge carried by both of these sites in the double phosphomimetic mutant interferes with the functions of the polybasic domain and alters the interaction of septins with the membrane in such a way that it causes the membrane to become unstable. If the membrane cannot be remodeled properly, the cell cannot grow. Another possibility for the dominant lethal effect is that the double point mutant interferes with the septins ability to scaffold a necessary signaling protein to the proper place during cell development. Because *Ashbya* Cdc12 S5E S8E has the same lethal effect when introduced to *S. cerevisiae*, the mislocalized protein would likely be a conserved factor. When only one of the sites is made phosphomimetic (Cdc12 S5D), the dominant lethal effect observed for the double point mutation is not phenocopied by the single (Table 6). This suggests that both sites must be negatively charged for lethality to occur, although it is also possible that Cdc12 S8D alone would be sufficient for the lethal phenotype. Remarkably, the opposite double mutant, Cdc12 S5A S8A, has no apparent cell or septin phenotypes, reinforcing the idea that specific charges on septin phosphorylation sites can make a dramatic difference in the functionality of the protein.

Another phosphomimetic mutant, Shs1 9D, is also lethal if it is expressed as the only copy of *SHS1* in the cell. Although this is not as extreme as the dominant lethality observed for Cdc12 S5E S8E, it is still quite astonishing. Because it is recessive lethal, we were able to observe the effects of the mutant protein expressed on a plasmid in cells where a wild-type copy of *SHS1* is present. Cells were healthy and septin rings appeared normal, however we observed that the Shs1 9D-GFP at IR rings was more dynamic than wildtype. Changes in septin dynamics correlated with the presence or absence of kinases or phosphatases have been previously reported in other systems (24, 31, 41); however, none of these studies directly assessed the affects of septin phosphorylation status on dynamics at the septin ring. We previously showed that the nonphosphorylatable mutant Shs1 9A-GFP does not have significantly altered dynamics at either IR or branch rings in *Ashbya* (25), so again we found that specific changes to septin phosphorylation sites direct septin functionality. It is unlikely that the increased dynamics of Shs1 9D alone are responsible for the mutant's lethal effects; however, it is possible that either decreased stability of septin structures as a result of increased turnover or changes in septin-septin or septin-membrane interactions caused by the mutation contribute to the lethality.

It is curious that the phosphomimetic *SHS1* allele leads to cell lethality, while the *SHS1*-null mutant is viable, although the null mutant is sick and does not assemble septin rings (19). Why would the complete absence of Shs1 be less deleterious than forcing nine sites on the protein to be phosphomimetic? One possibility is that the loss of Shs1p and septin rings leads to a decrease in proteins that are normally scaffolded by septins to their proper location. Perhaps some of the proteins can still arrive where they need to be stochastically, so the cells can survive, but they are not as healthy as they would be with an intact septin cytoskeleton. On the other hand, phosphomimetic Shs1p may be interacting too tightly with factors that wild-type Shs1p only interacts with transiently, leading to an accumulation of mislocalized protein, which could have a toxic effect. It will be interesting use the Shs1 9D protein expressed off a plasmid in *Ashbya* to assess whether it can stably bind to proteins that its wild-type counterpart does not.

We were surprised to discover that swapping the coiled-coil domain of Shs1p with that of Cdc11p resulted in the inability of the Shs1 chimera to incorporate into septin structures. Given that Shs1p with its coiled coil completely deleted is able to localize to the expanded ring structures characteristic of that mutant (25), it was puzzling that the Shs1-Cdc11 CC hybrid localized only to the cytoplasm. Intriguingly, Cdc11 readily localizes to septin structures in cells expressing the Shs1 chimeric protein, and these structures phenocopy the expanded branch rings and ectopic fibers witnessed in the Shs1p coiled-coil deletion mutants. A possible explanation for the exclusion of the chimeric protein at septin structures is that the Cdc11 coiled coil may be prohibiting lateral associations normally made by Shs1 to form rings (45). Evidently, the absence of the Shs1p coiled coil, even if replaced with another coiled coil, is sufficient to expand the septin branch structures beyond their normal boundaries. To put it another way, the Shs1p coiled coil specifically is required to limit septin ring size. It has been shown in *S. cerevisiae* that other septins localize to the ring at the mother-bud neck in *shs1*Δ cells, although the ring organization is abnormal (45, 46). It is possible that some similar mechanism is at work in *Ashbya*. The size or shape of the Cdc11p coiled coil appended to Shs1p may be prohibitive for the chimeric protein to associate with other septins or may prevent complexes that have the chimera from further assembling into longer polymers. In this case, septin complexes comprised of the other four septins would be the constituents of the septin rings, and the absence of the Shs1p coiled coil leads to the expanded septin structures.

In contrast to large assemblies forming, loss of the coiled coils of Cdc11p or Cdc12p eliminates nearly all higher-order structures. These phenotypes are very different from the Shs1p coiled-coil deletion and are even somewhat different from one another. Clearly, the Cdc11p and Cdc12p coiled coils do not act to limit septin ring size like that of Shs1p. The loss of the Cdc11p coiled coil results in a complete lack of septin structures. While Cdc12p coiled-coil deletion cells can infrequently assemble rings (7%), the remainder of these mutant cells display only cytoplasmic localization of Cdc12ΔCC-GFP, either diffusely or in small circles and crescents. Both of these mutants' phenotypes are consistent with the theory that the septin coiled coils are required for septin-septin interactions. Studies in yeast have revealed that coiled coils of Cdc11p, Cdc12p, and Cdc3p facilitate septin-septin interactions, and in the absence of these coiled coils, yeast cells have aberrant, elongated morphology and often fail to form normal septin rings (47, 48). Furthermore, one of the most widely used conditional mutants used in *S. cerevisiae*, *cdc12-6*, contains a C-terminal truncation (49). It will be interesting to dissect the differences between the septin coiled coils and how precisely they perform their apparently different cellular functions in future studies.

Overall, the data we present here delineate novel roles for septin phosphorylation and coiled-coil domains in regulating septin structure formation, as well as cell morphology and other functions. The specific mechanisms underlying the mutant phenotypes have yet to be described. It is possible that phosphorylation or lack thereof is important for masking or revealing certain parts of a given septin protein, allowing the septin to interact with another protein or with the membrane. Similarly, coiled coils may be influencing septin-septin or septin-membrane interaction. This study provides a first step toward understanding diverse effects of individual septin modifications and conserved domains and how these components may influence septin structure and function.

ACKNOWLEDGMENTS

We thank the Gladfelter lab for useful discussions.

This study is supported by National Science Foundation grant MCB-0719126 (awarded to A.S.G.) and National Institutes of Health training grant T32 AI007519 (awarded to R.A.M.).

REFERENCES

1. **Hartwell LH.** 1971. Genetic control of the cell division cycle in yeast. IV. Genes controlling bud emergence and cytokinesis. Exp. Cell Res. **69**:265–276.
2. **Nishihama R, Onishi M, Pringle JR.** 2011. New insights into the phylogenetic distribution and evolutionary origins of the septins. Biol. Chem. **392**:681–687.
3. **Pan F, Malmberg RL, Momany M.** 2007. Analysis of septins across kingdoms reveals orthology and new motifs. BMC Evol. Biol. **7**:103. doi: 10.1186/1471-2148-7-103.
4. **Barral Y, Mermall V, Mooseker MS, Snyder M.** 2000. Compartmentalization of the cell cortex by septins is required for maintenance of cell polarity in yeast. Mol. Cell **5**:841–851.
5. **Gladfelter AS, Pringle JR, Lew DJ.** 2001. The septin cortex at the yeast mother-bud neck. Curr. Opin. Microbiol. **4**:681–689.
6. **Hagiwara A, Tanaka Y, Hikawa R, Morone N, Kusumi A, Kimura H, Kinoshita M.** 2011. Submembranous septins as relatively stable components of actin-based membrane skeleton. Cytoskeleton (Hoboken) **68**: 512–525.

7. **Luedeke C, Frei SB, Sbalzarini I, Schwarz H, Spang A, Barral Y.** 2005. Septin-dependent compartmentalization of the endoplasmic reticulum during yeast polarized growth. J. Cell Biol. **169**:897–908.
8. **McMurray MA, Stefan CJ, Wemmer M, Odorizzi G, Emr SD, Thorner J.** 2011. Genetic interactions with mutations affecting septin assembly reveal ESCRT functions in budding yeast cytokinesis. Biol. Chem. **392**: 699–712.
9. **Takizawa PA, DeRisi JL, Wilhelm JE, Vale RD.** 2000. Plasma membrane compartmentalization in yeast by messenger RNA transport and a septin diffusion barrier. Science **290**:341–344.
10. **Ihara M, Yamasaki N, Hagiwara A, Tanigaki A, Kitano A, Hikawa R, Tomimoto H, Noda M, Takanashi M, Mori H, Hattori N, Miyakawa T, Kinoshita M.** 2007. Sept4, a component of presynaptic scaffold and Lewy bodies, is required for the suppression of alpha-synuclein neurotoxicity. Neuron **53**:519–533.
11. **Kinoshita A, Kinoshita M, Akiyama H, Tomimoto H, Akiguchi I, Kumar S, Noda M, Kimura J.** 1998. Identification of septins in neurofibrillary tangles in Alzheimer's disease. Am. J. Pathol. **153**:1551–1560.
12. **Peterson EA, Petty EM.** 2010. Conquering the complex world of human septins: implications for health and disease. Clin. Genet. **77**:511–524.
13. **Beise N, Trimble W.** 2011. Septins at a glance. J. Cell Sci. **124**:4141–4146.
14. **Oh Y, Bi E.** 2011. Septin structure and function in yeast and beyond. Trends Cell Biol. **21**:141–148.
15. **McMurray MA, Bertin A, Garcia G3rd, Lam L, Nogales E, Thorner J.** 2011. Septin filament formation is essential in budding yeast. Dev. Cell **20**:540–549.
16. **Field CM, al-Awar O, Rosenblatt J, Wong ML, Alberts B, Mitchison TJ.** 1996. A purified *Drosophila* septin complex forms filaments and exhibits GTPase activity. J. Cell Biol. **133**:605–616.
17. **Frazier JA, Wong ML, Longtine MS, Pringle JR, Mann M, Mitchison TJ, Field C.** 1998. Polymerization of purified yeast septins: evidence that organized filament arrays may not be required for septin function. J. Cell Biol. **143**:737–749.
18. **Bertin A, McMurray MA, Thai L, Garcia G3rd, Votin V, Grob P, Allyn T, Thorner J, Nogales E.** 2010. Phosphatidylinositol-4,5-bisphosphate promotes budding yeast septin filament assembly and organization. J. Mol. Biol. **404**:711–731.
19. **DeMay BS, Meseroll RA, Occhipinti P, Gladfelter AS.** 2009. Regulation of distinct septin rings in a single cell by Elm1p and Gin4p kinases. Mol. Biol. Cell **20**:2311–2326.
20. **Rodal AA, Kozubowski L, Goode BL, Drubin DG, Hartwig JH.** 2005. Actin and septin ultrastructures at the budding yeast cell cortex. Mol. Biol. Cell **16**:372–384.
21. **Amin ND, Zheng YL, Kesavapany S, Kanungo J, Guszczynski T, Sihag RK, Rudrabhatla P, Albers W, Grant P, Pant HC.** 2008. Cyclin-dependent kinase 5 phosphorylation of human septin SEPT5 (hCDCrel-1) modulates exocytosis. J. Neurosci. **28**:3631–3643.
22. **Egelhofer TA, Villen J, McCusker D, Gygi SP, Kellogg DR.** 2008. The septins function in G1 pathways that influence the pattern of cell growth in budding yeast. PLoS One **3**:e2022. doi:10.1371/journal.pone.0002022.
23. **Hernandez-Rodriguez Y, Momany M.** 2012. Posttranslational modifications and assembly of septin heteropolymers and higher-order structures. Curr. Opin. Microbiol. doi:10.1016/j.mib.2012.09.007.
24. **Li CR, Yong JY, Wang YM, Wang Y.** 2012. CDK regulates septin organization through cell-cycle-dependent phosphorylation of the Nim1-related kinase Gin4. J. Cell Sci. doi:10.1242/jcs.104497.
25. **Meseroll RA, Howard L, Gladfelter AS.** 2012. Septin ring size scaling and dynamics require the coiled-coil region of Shs1p. Mol. Biol. Cell **23**:3391–3406.
26. **Mitchell L, Lau A, Lambert JP, Zhou H, Fong Y, Couture JF, Figeys D, Baetz K.** 2011. Regulation of septin dynamics by the *Saccharomyces cerevisiae* lysine acetyltransferase NuA4. PLoS One **6**:e25336. doi:10.1371/journal.pone.0025336.
27. **Mortensen EM, McDonald H, Yates J3rd, Kellogg DR.** 2002. Cell cycle-dependent assembly of a Gin4-septin complex. Mol. Biol. Cell **13**:2091–2105.
28. **Sinha I, Wang YM, Philp R, Li CR, Yap WH, Wang Y.** 2007. Cyclin-dependent kinases control septin phosphorylation in *Candida albicans* hyphal development. Dev. Cell **13**:421–432.
29. **Tang CS, Reed SI.** 2002. Phosphorylation of the septin cdc3 in g1 by the cdc28 kinase is essential for efficient septin ring disassembly. Cell Cycle **1**:42–49.
30. **Xue J, Milburn PJ, Hanna BT, Graham ME, Rostas JA, Robinson PJ.** 2004. Phosphorylation of septin 3 on Ser-91 by cGMP-dependent protein kinase-I in nerve terminals. Biochem. J. **381**:753–760.
31. **Merlini L, Fraschini R, Boettcher B, Barral Y, Lucchini G, Piatti S.** 2012. Budding yeast dma proteins control septin dynamics and the spindle position checkpoint by promoting the recruitment of the Elm1 kinase to the bud neck. PLoS Genet. **8**:e1002670. doi:10.1371/journal.pgen.1002670.
32. **Sitz JH, Baumgartel K, Hammerle B, Papadopoulos C, Hekerman P, Tejedor FJ, Becker W, Lutz B.** 2008. The Down syndrome candidate dual-specificity tyrosine phosphorylation-regulated kinase 1A phosphorylates the neurodegeneration-related septin 4. Neuroscience **157**:596–605.
33. **Ayad-Durieux Y, Knechtle P, Goff S, Dietrich F, Philippsen P.** 2000. A PAK-like protein kinase is required for maturation of young hyphae and septation in the filamentous ascomycete *Ashbya gossypii*. J. Cell Sci. **113**(Pt 24):4563–4575.
34. **Wendland J, Ayad-Durieux Y, Knechtle P, Rebischung C, Philippsen P.** 2000. PCR-based gene targeting in the filamentous fungus *Ashbya gossypii*. Gene **242**:381–391.
35. **Altmann-Johl R, Philippsen P.** 1996. AgTHR4, a new selection marker for transformation of the filamentous fungus *Ashbya gossypii*, maps in a four-gene cluster that is conserved between *A. gossypii* and *Saccharomyces cerevisiae*. Mol. Gen. Genet. **250**:69–80.
36. **Helfer H, Gladfelter AS.** 2006. AgSwe1p regulates mitosis in response to morphogenesis and nutrients in multinucleated *Ashbya gossypii* cells. Mol. Biol. Cell **17**:4494–4512
37. **Sikorski RS, Hieter P.** 1989. A system of shuttle vectors and yeast host strains designed for efficient manipulation of DNA in *Saccharomyces cerevisiae*. Genetics **122**:19–27.
38. **Kaufmann A.** 2009. A plasmid collection for PCR-based gene targeting in the filamentous ascomycete *Ashbya gossypii*. Fungal Genet. Biol. **46**:595–603.
39. **Anker JF, Gladfelter AS.** 2011. Axl2 integrates polarity establishment, maintenance, and environmental stress response in the filamentous fungus *Ashbya gossypii*. Eukaryot. Cell **10**:1679–1693.
40. **Gladfelter AS, Hungerbuehler AK, Philippsen P.** 2006. Asynchronous nuclear division cycles in multinucleated cells. J. Cell Biol. **172**:347–362.
41. **Dobbelaere J, Gentry MS, Hallberg RL, Barral Y.** 2003. Phosphorylation-dependent regulation of septin dynamics during the cell cycle. Dev. Cell **4**:345–357.
42. **Gonzalez-Novo A, Correa-Bordes J, Labrador L, Sanchez M, Vazquez de Aldana CR, Jimenez J.** 2008. Sep7 is essential to modify septin ring dynamics and inhibit cell separation during *Candida albicans* hyphal growth. Mol. Biol. Cell **19**:1509–1518.
43. **Longtine MS, Fares H, Pringle JR.** 1998. Role of the yeast Gin4p protein kinase in septin assembly and the relationship between septin assembly and septin function. J. Cell Biol. **143**:719–736.
44. **Wightman R, Bates S, Amornrrattanapan P, Sudbery P.** 2004. In *Candida albicans*, the Nim1 kinases Gin4 and Hsl1 negatively regulate pseudohypha formation and Gin4 also controls septin organization. J. Cell Biol. **164**:581–591.
45. **Garcia G, 3rd, Bertin Li A, Song Z, McMurray Y, Thorner MA, Nogales JE.** 2011. Subunit-dependent modulation of septin assembly: budding yeast septin Shs1 promotes ring and gauze formation. J. Cell Biol. **195**: 993–1004.
46. **Iwase M, Luo J, Bi E, Toh-e, A.** 2007. Shs1 plays separable roles in septin organization and cytokinesis in *Saccharomyces cerevisiae*. Genetics **177**: 215–229.
47. **Casamayor A, Snyder M.** 2003. Molecular dissection of a yeast septin: distinct domains are required for septin interaction, localization, and function. Mol. Cell. Biol. **23**:2762–2777.
48. **Versele M, Gullbrand B, Shulewitz MJ, Cid VJ, Bahmanyar S, Chen RE, Barth P, Alber T, Thorner J.** 2004. Protein-protein interactions governing septin heteropentamer assembly and septin filament organization in *Saccharomyces cerevisiae*. Mol. Biol. Cell **15**:4568–4583.
49. **Li L, Zhang C, Konopka JB.** 2012. A *Candida albicans* temperature-sensitive *cdc12-6* mutant identifies roles for septins in selection of sites of germ tube formation and hyphal morphogenesis. Eukaryot. Cell **11**:1210–1218.
50. **Schmitz HP, Kaufmann A, Kohli M, Laissue PP, Philippsen P.** 2006. From function to shape: a novel role of a formin in morphogenesis of the fungus *Ashbya gossypii*. Mol. Biol. Cell **17**:130–145.